



A unified weighted minimum norm solution for the reference inverse problem in EEG

Ricardo A. Salido-Ruiz^a, Radu Ranta^{b,*}, Gundars Korats^c, Steven Le Cam^b, Laurent Koessler^{b,d}, Valerie Louis-Dorr^b

^a University of Guadalajara, Department of Computer Science in the University Center for Exact Sciences and Engineering (CUCEI), Guadalajara, Jalisco, Mexico

^b Université de Lorraine, CNRS, CRAN, F-54000 Nancy, France

^c Ventspils University of Applied Sciences, Ventspils Smart Technology Research Centre, Ventspils, Latvia

^d CHRU Nancy, Neurology Department, Epilepsy Unit F-54000 Nancy, France

ARTICLE INFO

Keywords:

EEG

Reference potential

Inverse problems

ABSTRACT

A well known problem in EEG recordings deals with the unknown potential of the reference electrode. In the last years several authors presented comparisons among the most popular solutions, the global conclusion being that the traditional Average Reference (AR) and the Reference Standardization Technique (REST) are the best approximations (Nunez, 2010; Kayser and Tenke, 2010; Liu et al., 2015; Chella et al., 2016). In this work we do not aim to further compare these techniques but to support the fact that both solutions can be derived from a general inverse problem formalism for reference estimation (Hu et al., 2019; Hu et al., 2018; Salido-Ruiz et al., 2011). Using the alternative approach of least squares, our findings are consistent with the theoretical findings in Hu et al. (2019) and Hu et al. (2018) showing that the AR is the minimum norm solution, while REST is a weighted minimum norm including some approximate propagation model. AR is thus a particular case of REST, which itself uses a particular formulation of the source estimation inverse problem. With a different derivation, we provide the additional powerful evidences to reinforce the cited findings.

1. Introduction

The EEG signals measure the potential difference between an electrode, placed somewhere on the head surface, and a reference electrode, placed somewhere else on the body. Ideally, the reference electrode should be placed in the most electrically inactive position and far from the region of interest. In practice, the reference is contaminated with unknown local and/or propagated electrical activity. Still, most of the studies need reference free potentials for better results [4–8]. For example, functional brain connectivity are estimated using coherence and phase delays among EEG channels, and the reference potential might strongly affect these methods¹ [8–12]. A previous study showed that even Blind Source Separation techniques might be affected by the reference problem [13].

This paper focuses on EEG recorded using a scalp reference. In this case, the reference electrode captures the same kind of activity as any other electrode, that is a mixture of brain sources. In this

context, the most popular solution for canceling the reference potential is to subtract the spatial average of the recorded signals from all measurements. This solution, known as average reference montage (AR) was challenged by the Reference Standardization Technique (REST) [6]. Several authors compared the two solutions (or other re-referencing techniques) [7,14–19], the overall conclusion being that REST is deemed to yield better results, although this is not always the case, especially when the head model is prone to inaccuracies. The goal of this paper is to theoretically show that both AR and REST belong to the same family of inverse problems widely encountered in EEG analysis, *i.e.*, weighted minimum norms. Although the same idea was recently put forward by [20,21] by matrix differential calculus and maximum a posterior estimation, our paper proposes an alternative simple algebraic proof (another algebraic proof can be found also in [17], in French). To avoid redundancies with the previously cited papers, we do not present extensive simulation results comparing classical AR and REST solutions. Instead, we focus on different (REST-like)

* Corresponding author.

E-mail addresses: ricardo.salido@cucei.udg.mx (R.A. Salido-Ruiz), radu.ranta@univ-lorraine.fr (R. Ranta).

¹ Although some of these studies were focused on intracranial EEG, the effect of the reference potential is the same. Note though that for iEEG, the reference estimation techniques are different, as they assume that the reference is sufficiently far from the measuring electrodes to be considered independent/uncorrelated [1–3].

versions of weighted minimum norm solutions, including equivalent sources distributed in the whole head volume or on dipolar layers at different positions around the brain. The accuracy of these different solutions is evaluated with respect of the degree of precision that one can inject in the inversion model, based on some *a priori* knowledge.

2. EEG Measurement model

Consider the classical EEG linear model given by:

$$\mathbf{x} = \mathbf{A}\mathbf{s} \quad (1)$$

where $\mathbf{x} \in \mathbb{R}^{m \times 1}$ is a vector with unknown real potentials under each electrode with respect to infinity, from here defined as absolute potentials for the m electrodes, $\mathbf{A} \in \mathbb{R}^{m \times p}$ is the mixing lead-field matrix and $\mathbf{s} \in \mathbb{R}^{p \times 1}$ is the source vector. Note that the reference potential is included among the m ; for convenience, it will be assumed in the rest of the paper that this potential is the m th one. In EEG, the matrix \mathbf{A} represents the head model, obtained either by analytical approximations (e.g. spherical head models) or numerically, for realistic head models obtained after MRI segmentation of head structures (brain, CSF, skull, scalp). The sources vector \mathbf{s} contains the amplitudes of the dipoles that model the neural sources [22]. For these realistic models, possible source emplacements depend on the brain volume discretization but, regardless of the used head model, the number of sources p is far bigger than the number of electrodes m ($p \gg m$). Eq. (2) introduces the so-called instantaneous mixture model, with the matrix \mathbf{A} time-invariant and of rank m . For real signals recorded in time having $n > m$ time samples, the vectors \mathbf{x} and \mathbf{s} become matrices of dimension $m \times n$ and $p \times n$ respectively:

$$\mathbf{X} = \mathbf{A}\mathbf{S} \quad (2)$$

Note that we consider during all the paper that the ideal infinity-referenced data matrix \mathbf{X} has linearly independent rows, thus it is rank m . This of course can only be true if the rank of the source matrix \mathbf{S} is greater or equal to m , i.e., if there are at least m linearly independent sources.

The actually measured potentials are given by the common reference montage (CR), with potentials \mathbf{X}_{CR} modeled by subtracting the potential of the chosen reference electrode from the other electrodes. This can be seen as a matrix transform of the absolute potentials from (2):

$$\mathbf{X}_{CR} = \mathbf{T}_{CR}\mathbf{x} = \mathbf{T}_{CR}\mathbf{A}\mathbf{s} = \mathbf{A}_{CR}\mathbf{s} \quad (3)$$

with \mathbf{T}_{CR} the $m - 1$ rank matrix:

$$\mathbf{T}_{CR} = \begin{bmatrix} \mathbf{I}_{m-1} & -\mathbf{1}_{m-1} \end{bmatrix} \quad (4)$$

where \mathbf{I}_{m-1} is the $(m - 1) \times (m - 1)$ identity matrix and $\mathbf{1}_{m-1} \in \mathbb{R}^{(m-1) \times 1}$ is a vector of 1's. As mentioned above and with no loss of generality, we assume the reference electrode potential as the last absolute potential in EEG linear model (2). Note that, unlike \mathbf{X} in (2), the dimension of \mathbf{X}_{CR} is $m - 1 \times n$ (number of available signals).

The most employed solutions propose to cancel the reference by transforming the CR into other EEG montages (average reference — AR, bipolar — BM, Laplacian — LapM) [1,4,14,23,24]. A more elaborated solution, based on head modeling, is the reference standardization (REST) [6]. Among these, only AR and REST propose absolute potential estimations, the BM and the LapM being local estimators (along with the reference potential, they also cancel propagated activities originating in far situated regions [25]). We will only focus here on the former.

2.1. Average reference (AR)

The classical rationale behind average reference montages (AR) is that, under the hypothesis of equidistributed electrodes covering the whole head, the sum of all electrode potentials on the scalp should be zero (see [26] for a proof for the spherical head model).

In practice, as the only available signals are \mathbf{x}_{CR} , AR signals are obtained by calculating the sum of the $m - 1$ \mathbf{x}_{CR} signals, dividing it by the total number of electrodes m and subtracting it from each measurement [5,27,28]. More formally, the AR is obtained by averaging over all electrodes (reference electrode included with a null potential (i.e., its potential with respect to itself):

$$\mathbf{X}_{AR} = \left(\mathbf{I}_m - \frac{1}{m} \mathbf{1}_m \mathbf{1}_m^T \right) \begin{bmatrix} \mathbf{X}_{CR} \\ 0 \end{bmatrix} = \mathbf{T}_{AR} \mathbf{X}_{CR} \quad (5)$$

with

$$\mathbf{T}_{AR} = \begin{bmatrix} \mathbf{I}_{m-1} - \frac{1}{m} \mathbf{1}_{m-1} \mathbf{1}_{m-1}^T \\ -\frac{1}{m} \mathbf{1}_{m-1}^T \end{bmatrix} \quad (6)$$

As we can see, \mathbf{X}_{AR} has a dimension of $m \times n$ and rank of $m - 1$, i.e., it preserves the rank of \mathbf{X}_{CR} (one less than \mathbf{X}). In practice, the average signal is included as the last row of \mathbf{X}_{AR} , noted for convenience ($\mathbf{x}_{m,AR}$).²

2.2. Reference electrode standardization technique (REST)

The REST method [6,14] allows to estimate absolute potentials at any point on the scalp by solving a forward problem with “equivalent sources” $\tilde{\mathbf{s}}$ constrained to a dipolar layer completely surrounding the actual sources, i.e., the brain. Several versions can be theoretically proposed, depending on the configuration chosen for the dipolar layer (e.g., a sphere circumscribing the whole brain, or the numerically approximated cortical surface). The chosen dipolar layer will yield a specific forward model between the dipoles situated on this layer and the actual electrodes placed on the head surface. Let this model be $\tilde{\mathbf{A}}$. The equivalent dipolar sources on this layer are estimated from scalp EEG recordings (equivalently in CR or in AR) by using a simple inverse problem formalism. We give below only the CR based approach:

$$\hat{\tilde{\mathbf{S}}} = \tilde{\mathbf{A}}_{CR}^+ \mathbf{X}_{CR} \quad (7)$$

with $^+$ designating the classical Moore–Penrose pseudo-inverse. Of course, $\tilde{\mathbf{A}}_{CR}$ depends on a mixing model (see Eq. (4)), here assumed $\tilde{\mathbf{A}}$. A forward model using the assumed $\tilde{\mathbf{A}}$ and the estimated equivalent sources $\hat{\tilde{\mathbf{S}}}$ yields the REST estimations of the EEG absolute potentials:

$$\mathbf{X}_{REST} = \tilde{\mathbf{A}} \hat{\tilde{\mathbf{S}}} = \tilde{\mathbf{A}} \tilde{\mathbf{A}}_{CR}^+ \mathbf{X}_{CR} = \mathbf{T}_{REST} \mathbf{X}_{CR} \quad (8)$$

It is important to recall that different REST solutions can be obtained by choosing different dipolar layer configurations and thus different $\tilde{\mathbf{A}}$ models.

3. Unified inverse problem modeling

As seen above, two main solutions exist for estimating the absolute potentials: average montage and REST. Three relatively recent comparative studies [7,16,18] conclude that both solutions present valid theoretical arguments and that both are acceptable. Our aim is to deepen the analysis, to show the connections between the two techniques and their integration in a larger inverse problem framework.

² Note that in [19], the formulation is done differently (i.e., they use a \mathbf{T}_R of dimension $N_e \times N_e$, $m = N_e$ in our case), but they are equivalent (i.e., one of the rows of \mathbf{T}_R has only zeros). Our rationale was to start, as in classical inverse problems, from the actual measurements \mathbf{X}_{CR} and not from the absolute potentials. Still, the two formulations yield the same conclusions.

Consider the case of a EEG recording with a cephalic reference as given in (Eq. (3)). The estimation of absolute potentials \mathbf{x} from the measured \mathbf{x}_{CR} and matrix transformation \mathbf{T}_{CR} , is an ill-posed inverse problem somehow similar to the classical EEG source estimation with a known mixing model \mathbf{T}_{CR} .

Thus, the absolute potentials inverse problem writes as follows:

$$\hat{\mathbf{X}} = \mathbf{T}\mathbf{x}_{CR} = \mathbf{T}\mathbf{T}_{CR}\mathbf{x} \quad (9)$$

where the unknown matrix $\mathbf{T} \in \mathbb{R}^{m \times m-1}$ is a generalized inverse of the common reference transformation matrix \mathbf{T}_{CR} :

$$\mathbf{T} = \mathbf{W}^{-1}\mathbf{T}_{CR}^T [\mathbf{T}_{CR}\mathbf{W}^{-1}\mathbf{T}_{CR}^T]^{-1} \quad (10)$$

with \mathbf{W} a weighting matrix allowing infinite solutions. In the next paragraphs we describe several particular Weighted Minimum Norm (WMN) solutions.

3.1. WMN optimal solution: Oracle1

The underdetermined system (9) has an infinite number of solutions. In theory, the best inverse transform \mathbf{T} can be estimated by minimizing the least-squares error between absolute and measured potentials. This optimal transform \mathbf{T}_{O1} can be obtained by multiplying absolute potentials \mathbf{x} by the Moore–Penrose pseudo inverse of measured potentials matrix \mathbf{X}_{CR} :

$$\mathbf{T}_{O1} = \mathbf{X}\mathbf{X}_{CR}^T [\mathbf{X}_{CR}\mathbf{X}_{CR}^T]^{-1} = \mathbf{A}\Sigma_s\mathbf{A}^T\mathbf{T}_{CR}^T [\mathbf{T}_{CR}\mathbf{A}\Sigma_s\mathbf{A}^T\mathbf{T}_{CR}^T]^{-1} \quad (11)$$

where \mathbf{A} the head model and $\Sigma_s = \mathbf{S}\mathbf{S}^T$ is the source scatter matrix (for completeness, the proof is given in the appendix). This optimal solution is equivalent to (10) for $\mathbf{W}^{-1} = \Sigma_x = \mathbf{A}\Sigma_s\mathbf{A}^T$ ($\Sigma_x = \mathbf{X}\mathbf{X}^T$ being the scatter matrix of the absolute potentials). Of course, it remains theoretical, because neither the absolute potentials scatter matrix nor, equivalently, the propagation coefficients between the actual sources \mathbf{S} and the sensors (depending on the sources positions and orientations and on the head model) and the source scatter matrix, are known in practice.³

3.2. WMN sub-optimal solutions: Oracle2 and REST

In practice, Σ_s is not known and prior covariance matrices $\hat{\Sigma}_s$ are difficult to construct. On the other hand, rather accurate head models can be obtained for \mathbf{A} for all possible source locations inside the brain volume.

Ignoring the source amplitudes (or their covariance matrix) but supposing that we have some *a priori* knowledge on their positions and orientations, as well as a good head model (i.e., making $\Sigma_s = \mathbf{I}_p$ but assuming a known \mathbf{A}), one obtains:

$$\begin{aligned} \mathbf{T}_{O2} &= \mathbf{A}\mathbf{A}^T\mathbf{T}_{CR}^T [\mathbf{T}_{CR}\mathbf{A}\mathbf{A}^T\mathbf{T}_{CR}^T]^{-1} \\ &= \mathbf{A} [\mathbf{T}_{CR}\mathbf{A}]^+ = \mathbf{A}\mathbf{A}_{CR}^+ \end{aligned} \quad (12)$$

A step further towards more realistic situations is to ignore the source positions and orientations, but to still assume a complete head model, i.e., a mixing matrix \mathbf{A}_C corresponding to a complete lead-field matrix for all possible source configurations (of course, in practice it will be computed for a grid of points inside the brain volume). The equations are exactly the same as (12), with a complete mixing matrix \mathbf{A}_C replacing \mathbf{A} (which is an incomplete lead-field matrix, in the sense that it accounts only for the *a priori* known source positions and orientations). Finally, as pointed out in [6], distributing equivalent sources on a

layer surrounding the actual brain sources, theoretically yields another mixing model \mathbf{A}_R used in the REST solution.

If Oracle1 and Oracle2 cannot be used in practice (because they are based on unknown information on the actual sources), it is noteworthy that REST-like solutions (either based on a complete volume model or an equivalent layer) could be in principle used, because they only need a propagation model between some chosen sources and the surface electrodes, and these models can be estimated with more or less accuracy from imaging techniques and physical considerations (see e.g. [29] for a review of the forward problem in EEG)).

Finally, it is easy to see that all these weighted minimum norm solutions share the same equation (12), which enlightens the fact that any full-rank matrix $\tilde{\mathbf{A}}$ can be used to construct a generalized inverse of \mathbf{T}_{CR} . Indeed,

$$\mathbf{T}_{CR}\tilde{\mathbf{A}}\tilde{\mathbf{A}}^T\mathbf{T}_{CR}^T [\mathbf{T}_{CR}\tilde{\mathbf{A}}\tilde{\mathbf{A}}^T\mathbf{T}_{CR}^T]^{-1} = \mathbf{I}_{m-1}$$

regardless of the accuracy of the model $\tilde{\mathbf{A}}$. In this sense, a completely false or random model $\tilde{\mathbf{A}}$ will yield false estimates of the absolute potentials $\hat{\mathbf{X}}$, but they will still verify the measured common reference signals $\mathbf{X}_{CR} = \mathbf{T}_{CR}\hat{\mathbf{X}}$.

3.3. Minimum norm solution, MN

Within this context, the most evident solution of (10), without any *a priori* information about the mixture or the sources (i.e., neither on \mathbf{A} nor on the source covariance), is the Minimum Norm Solution (MN) obtained when $\mathbf{W} = \mathbf{I}_m$. Then, an estimation of absolute potentials is given by:

$$\begin{aligned} \hat{\mathbf{x}} &= \mathbf{T}_{CR}^T (\mathbf{T}_{CR}\mathbf{T}_{CR}^T)^{-1} \mathbf{x}_{CR} \\ &= \mathbf{T}_{CR}^+ \mathbf{x}_{CR} \end{aligned} \quad (13)$$

with \mathbf{T}_{CR}^+ the Moore–Penrose pseudo-inverse of the common reference transformation matrix \mathbf{T}_{CR} .

Proposition. *The minimum norm solution to the inverse reference problem is the AR solution from (6):*

$$\mathbf{T}_{CR}^+ = \mathbf{T}_{AR}$$

Proof. By Sherman–Morrison formula and using the definition of the Moore–Penrose pseudo-inverse and the expression of \mathbf{T}_{CR} (4), one can write:

$$\begin{aligned} \mathbf{T}_{CR}^+ &= \mathbf{T}_{CR}^T (\mathbf{T}_{CR}\mathbf{T}_{CR}^T)^{-1} \\ &= \begin{bmatrix} \mathbf{I}_{m-1} \\ -\mathbf{1}_{m-1}^T \end{bmatrix} \left(\begin{bmatrix} \mathbf{I}_{m-1} & -\mathbf{1}_{m-1} \end{bmatrix} \begin{bmatrix} \mathbf{I}_{m-1} \\ -\mathbf{1}_{m-1}^T \end{bmatrix} \right)^{-1} \\ &= \begin{bmatrix} \mathbf{I}_{m-1} \\ -\mathbf{1}_{m-1}^T \end{bmatrix} [\mathbf{I}_{m-1} + \mathbf{1}_{m-1}\mathbf{1}_{m-1}^T]^{-1} \\ &= \begin{bmatrix} \mathbf{I}_{m-1} \\ -\mathbf{1}_{m-1}^T \end{bmatrix} \left(\mathbf{I}_{m-1} - \mathbf{1}_{m-1} \frac{\mathbf{1}_{m-1}^T}{1 + \mathbf{1}_{m-1}^T \mathbf{1}_{m-1}} \right) \\ &= \begin{bmatrix} \mathbf{I}_{m-1} \\ -\mathbf{1}_{m-1}^T \end{bmatrix} \left(\mathbf{I}_{m-1} - \mathbf{1}_{m-1} \frac{1}{m} \mathbf{1}_{m-1}^T \right) \\ &= \mathbf{T}_{AR} \end{aligned} \quad (14)$$

In the first row, we use block-matrix multiplication, while in the second we use the Sherman–Morrison formula (or more generally the Woodbury identity), see for example [30]). Readers interested by a second algebraic proof are directed to [17].

Note that the AR montage obtained by pseudo-inverting \mathbf{T}_{CR} can be seen as another particular case of REST, obtained for a dipolar layer having the head geometry and situated infinitely close below the electrodes (closely mimicking an $\tilde{\mathbf{A}} = \mathbf{I}_m$).

³ Note that, if some *a priori* knowledge on the spatial covariance of the sources are available, the source scatter matrix can be replaced by the hypothesized covariance matrix $\hat{\Sigma}_s$. The minimum norm solution will then be equivalent to the maximum likelihood estimation under a Gaussian hypothesis on the spatial source distribution $p(\mathbf{S}) = \mathcal{N}(\mathbf{0}, \hat{\Sigma}_s)$.

4. Results

The aim of this section is to briefly present numerical results, both on simulated and real data, supporting the previous analysis.

4.1. Simulation

The simulations presented here illustrate the fact that the accuracy of different estimations of the absolute potentials, obtained using the previously described approaches. These estimated potentials are compared with simulated ground truth potentials, computed as follows: a three shell mesh model (Colin 27) was extracted from Brainstorm [31] toolbox in order to have a realistic geometry. The cortical layer mesh (inner shell) had 642 nodes with 13 mm mean distance between neighboring points, while the scalp mesh (outer shell) had 1922 nodes.

A regularly spaced grid was constructed inside the inner shell (brain), with a 13 mm distance between neighboring points, which yielded 1774 points. Several source configurations were tested, namely using $p = \{128, 256, 512, 1024\}$ dipolar brain sources randomly chosen among the inner shell grid points. The orientations were random, and the time courses were simulated as spatially and temporally correlated Gaussians of length $N_s = \left(\frac{m}{8} + 1\right) \times f_s$ seconds (rule derived from [32]), f_s being sampling frequency and m the number of scalp electrodes. Three sensor setups were tested using $m = \{64, 128, 256\}$ scalp electrodes placed on the head surface (outer shell) according to the 10–10 system, one of them being the reference electrode. Sensor coordinates were also extracted from the Brainstorm toolbox and *snapped* to the mesh vertices by nearest-neighbor rule. The absolute EEG scalp potentials were simulated by projecting the sources of interest to the sensors using the BEM model implemented in the Helsinki toolbox [33], with conductivity ratios of 40:1 between the brain and the skull and 1:1 between brain and scalp. Simulated absolute potentials \mathbf{X} were transformed into measured potentials \mathbf{X}_{CR} by (3). One hundred simulations were performed for every configuration (position, orientations and time courses of the dipoles).

In order to evaluate the influence of the **model accuracy** on the results, we implemented different weighted inverse solutions, from the fully specified Oracle (11) to the model-free average reference (5), passing through REST and volume $REST_v$ (12). For $REST_v$, the lead-field \mathbf{A}_C was computed for the complete grid of 1774 volume points inside the brain shell and all three orientations ($m \times 5322$). For REST, the lead-field \mathbf{A} was computed for the cortical layer of 642 points and for dipoles orthogonal to the scalp ($m \times 642$). For completeness, we also implemented a REST-like solution, in which we used a random \mathbf{A} mixing model ($m \times 642$, generated as a spatially correlated uniform random variables), with no physical significance. We re-emphasize here that all models (including the random one) perfectly explain the CR measurements.

The evaluation criterion was the relative error introduced in [6]:

$$RE = \|\mathbf{X} - \hat{\mathbf{X}}\| / \|\mathbf{X}\| \quad (15)$$

where \mathbf{X} contains the absolute potentials, $\hat{\mathbf{X}}$ are the estimates and $\|\cdot\|$ is the Frobenius norm.

The simulation results (Table 1) confirm the hypothesis that the accuracy of the estimated zero-referenced potentials is proportional to the amount of additional correct information injected in the solution. In principle, one should use as complete models as possible.⁴

If we put aside the Oracles, very accurate but impossible to use in practice, the complete full-volume $REST_v$ model generally outperforms the cortical REST, at least for the same spatial density of the lead-field matrix (not shown here, a denser cortical layer REST also improves the estimations). When comparing classical REST and AR estimates, the

Table 1

Simulation results (Relative Error (15)) for different numbers of active brain sources and sensors configurations. The results (mean and standard deviations) are obtained on 100 simulations with random positioned sources of random amplitudes and orientations.

| | | RE_o | RE_{o2} | RE_{REST_v} | RE_{REST} | RE_{AR} | RE_{rand} |
|--------------|-------|--------|-----------|---------------|-------------|-----------|-------------|
| 64 sensors | | | | | | | |
| 100 sources | Mean | 0.04 | 0.06 | 0.17 | 0.22 | 0.24 | 20.39 |
| | (std) | (0.01) | (0.02) | (0.04) | (0.12) | (0.04) | (6.49) |
| 250 sources | Mean | 0.08 | 0.10 | 0.17 | 0.26 | 0.25 | 20.73 |
| | (std) | (0.02) | (0.03) | (0.03) | (0.14) | (0.04) | (7.55) |
| 500 sources | Mean | 0.10 | 0.11 | 0.16 | 0.32 | 0.26 | 20.92 |
| | (std) | (0.02) | (0.02) | (0.03) | (0.14) | (0.03) | (5.92) |
| 1000 sources | Mean | 0.12 | 0.13 | 0.16 | 0.34 | 0.26 | 20.83 |
| | (std) | (0.02) | (0.02) | (0.02) | (0.11) | (0.03) | (7.56) |
| 128 sensors | | | | | | | |
| 100 sources | Mean | – | – | 0.16 | 0.22 | 0.32 | 4.29 |
| | (std) | – | – | (0.04) | (0.13) | (0.04) | (1.38) |
| 250 sources | Mean | 0.06 | 0.09 | 0.17 | 0.25 | 0.31 | 4.42 |
| | (std) | (0.01) | (0.02) | (0.04) | (0.12) | (0.03) | (1.26) |
| 500 sources | Mean | 0.10 | 0.12 | 0.16 | 0.28 | 0.31 | 4.29 |
| | (std) | (0.02) | (0.02) | (0.03) | (0.11) | (0.02) | (1.24) |
| 1000 sources | Mean | 0.12 | 0.14 | 0.16 | 0.31 | 0.31 | 4.45 |
| | (std) | (0.02) | (0.02) | (0.02) | (0.10) | (0.02) | (1.21) |
| 256 sensors | | | | | | | |
| 100 sources | Mean | – | – | 0.15 | 0.22 | 0.31 | 3.75 |
| | (std) | – | – | (0.04) | (0.11) | (0.04) | (1.36) |
| 250 sources | Mean | – | – | 0.15 | 0.23 | 0.30 | 3.60 |
| | (std) | – | – | (0.03) | (0.10) | (0.03) | (1.09) |
| 500 sources | Mean | 0.05 | 0.08 | 0.14 | 0.27 | 0.30 | 3.76 |
| | (std) | (0.01) | (0.02) | (0.03) | (0.10) | (0.02) | (1.16) |
| 1000 sources | Mean | 0.08 | 0.10 | 0.14 | 0.31 | 0.30 | 3.90 |
| | (std) | (0.01) | (0.02) | (0.02) | (0.09) | (0.02) | (1.23) |

former are in average more performant. Still, this is not the case for low density montages and high number of sources, i.e., when the number of active sources is much higher than the number of sensors. More precisely, REST performances are stable with respect to the number of sensors, but they slightly degrade when the number of sources increases, while the AR estimates remain mostly unaffected by the number of active brain sources (although they seem to be better for the 64 sensors montage than for higher density ones). Interestingly, REST performances have a higher variance than AR based ones, regardless of the configuration. Finally, completely wrong models (random \mathbf{A}) yield the worst solutions, far below the average reference AR.

Fig. 1 graphically presents simulation results for a head model with 512 dipolar brain sources and 64, 128 and 256 electrodes (the random configuration is not presented).

4.2. Real signals

According to our previous argumentation, REST and AR solutions should converge to the same solution when the dipolar layer used for REST approaches the head surface and thus the sensors. We have evaluated their relationship using real data, without any previous knowledge on the sources. The EEG signals (resting state) were recorded in the epilepsy unit of the University Hospital of Nancy during routine clinical evaluation of an epileptic patient. Patient gave his/her informed consent for this study. This patient (25 year-old woman) had a normal MRI (i.e. without visible MR lesion) and insulo-opercular epilepsy. Seventy-six electrodes were placed according to the 10–10 system [34], the reference electrode being chosen, for clinical reasons at FPz. The head model (scalp, outer skull, inner skull) were computed from the MRI of the patient using the BrainStorm pipeline (1922 nodes and 3840 faces for each surface).

⁴ Note that Oracle solutions cannot function if the number of sources is below the number of sensors because of the matrix inversion in (11) and (12).

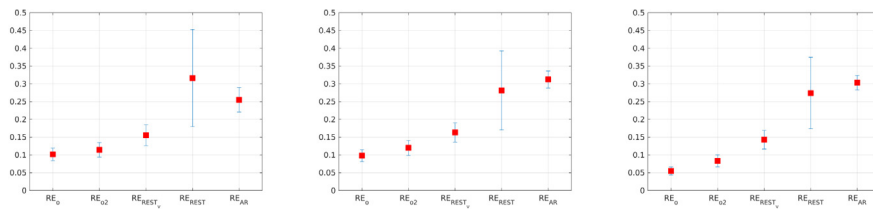


Fig. 1. Relative errors RE . The red dots represent mean values over 100 simulations, the standard deviations being given by the vertical whiskers. Only the 500 sources configurations are shown here (from left to right, 64, 256 and 256 sensors). Complete simulation results are given in Table 1.

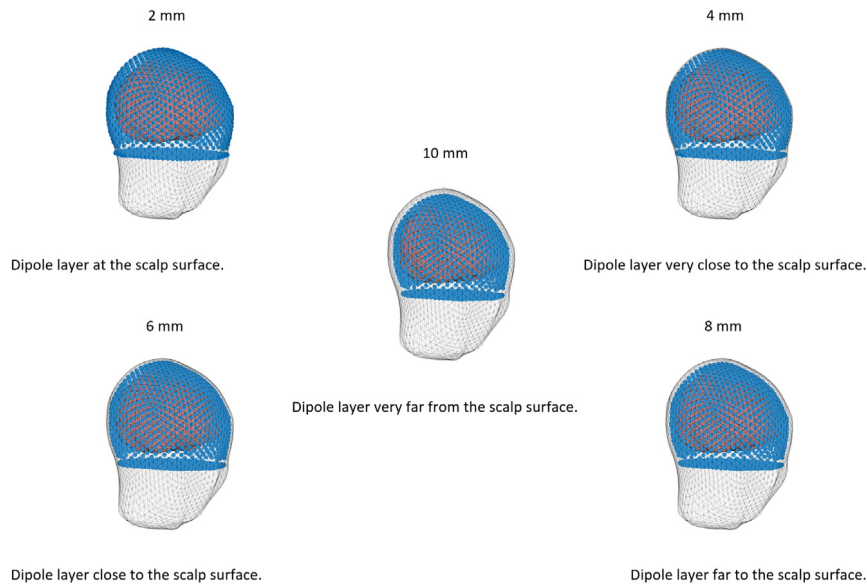


Fig. 2. Partial head mesh for the studied epileptic patient. To ease the visualization, only the scalp (in gray) and the inner skull (in red) are represented, along with the dipolar layer (in blue) used for REST (here at 2 mm, 4 mm, 6 mm and 8 mm depth below the scalp surface). (For interpretation of the references to color in this figure legend, the reader is referred to the web version of this article.)

Table 2

Relative error between the AR and REST estimations, depending on the depth of the dipolar layer.

| Depth | 10 mm | 8 mm | 6 mm | 4 mm | 2 mm |
|-------|--------|--------|--------|--------|--------|
| RE | 0.0537 | 0.0387 | 0.0211 | 0.0063 | 0.0057 |

Several REST solutions were computed for the absolute potentials, for dipolar layers placed at different depths (2 mm, 4 mm, 6 mm, 8 mm and 10 mm) with respect to the head surface, but outside the brain (inner skull) mesh (see Fig. 2). The geometry of the layer was the same as the one of the scalp, in order to be able to keep a constant distance between the sensors and the layer, except in the lower part of the brain, where we considered a flat surface 10 mm outside the inner skull. The number of dipoles on the layer was constant and the same as the number of points on the scalp mesh (1922).

We used the same criterion RE for evaluating the difference between REST and AR montages, REST being considered the ground truth (X in (15)) and AR the estimate \hat{X} . The results are given in Table 2, for different depths of the dipolar layer. As it can be seen, the closer the dipolar layer to the surface, the smaller the “distance” (the relative difference, in Frobenius norm) between the AR and REST estimates. It is useful to note that, for the real signals, as there is no ground truth, it is impossible to strictly evaluate the performances of the different solutions. The aim of this section is to highlight the fact that the AR montage is a limit case of the surface-based REST, when the layer is close to the head surface. On the other hand, if the layer is too deep

(below the brain surface), it will miss cortical sources and the estimate of the absolute reference montage (using REST) will be theoretically false.

5. Discussion

This work presents a unified inverse problem framework for the reference problem in (sensor noise free) surface EEG, which is an algebraic alternative to the approach recently proposed by [19–21]. This algebraic least-squares (LS) solution is common when an inverse problem has no exact solution and it can be extended to the general linear inverse problem as presented in [35]. The solution to general linear inverse problems from the point of view of LS is the Moore–Penrose pseudo-inverse, leading to minimum norm and weighted minimum norm solutions [36–38]. In the EEG case we are interested in, the absolute potentials estimation by pseudo-inversion is an underdetermined inverse problem, as the number of absolute potentials to be estimated is greater than the number of available signals (m with respect to $m - 1$ in the notations used in this paper). Consequently, the problem has an infinite number of solutions, parametrized by the *a priori* information that can be injected. The different parametrizations lead to different so-called *Weighted* MN solutions, having different accuracies depending on the quality of the injected *a priori* information, as we have shown in the previous section.

Among these solutions, the ideal *Oracle* involves some priors on the absolute potentials (or brain sources) covariance. On the other hand, the other proposed solutions are based only on linear algebra

(i.e., they are weighted minimum norms with deterministic weight matrices). In the recent literature, Hu et al. adopt matrix differential calculus and best linear unbiased estimator to the underdetermined linear regression problem in [21], and maximum posteriori or penalized likelihood estimates to the Bayesian linear inverse problem in [20] which are common in solving the inverse solution in the field of the electrophysiology source imaging. With a different derivation, the results we present here are similar to the theoretical findings in [20,21].

Finally, we have to note that even if the developments here were presented for monopolar reference EEG (which is the most current recording setup), they can easily be extended to other montages, such as linked mastoids. Indeed, this situation could be modeled by replacing the -1 column in the \mathbf{T}_{CR} (4) by two columns of -0.5 and changing the dimension of the \mathbf{I}_{m-1} identity matrix (to \mathbf{I}_{m-2}). The measured potentials will be modeled by multiplying this \mathbf{T}_{LM} linked-mastoids transform with the absolute potentials (including, on the last 2 rows, the potentials of the two mastoids). The derivation of the pseudo-inverse of this follows the same steps as above (14), yielding estimates of the absolute potentials.

6. Conclusions

As mentioned, our aim is not to present new simulation results, for extensive simulation results and comparisons (including the effects of model errors, geometry or noise errors), the reader is referred to [7,14–16,18,39]. The main contribution of the work presented in this paper is the reformulation of different reference estimation methods. Indeed, all methods, from the best possible model based *Oracle1* to the model-free average reference, can be seen as ill-posed inverse problems aiming to estimate absolute potentials from the measurements. In particular, we have shown that the AR is the minimum-norm solution to this problem, while the other methods are weighted norms, more or less accurate depending on the amount and on the precision of the injected *a priori* information.

Declaration of competing interest

The authors declare that they have no known competing financial interests or personal relationships that could have appeared to influence the work reported in this paper.

Acknowledgments

The authors would like to thank for the funding to the National Council of Science and Technology of Mexico (CONACyT) and the Latvian National Research Programme “The next generation of information and communication technologies” (NexIT).

Appendix

Demonstration of \mathbf{T}_O

$$\begin{aligned}
 \mathbf{T}_O &= \mathbf{x}\mathbf{x}_{CR}^T [\mathbf{x}_{CR}\mathbf{x}_{CR}^T]^{-1} \\
 &= \mathbf{x}\mathbf{x}_{CR}^T \mathbf{T}_{CR}^T [\mathbf{T}_{CR}\mathbf{x}\mathbf{x}_{CR}^T \mathbf{T}_{CR}^T]^{-1} \\
 &= \mathbf{\Sigma}_x \mathbf{T}_{CR}^T [\mathbf{T}_{CR}\mathbf{\Sigma}_x \mathbf{T}_{CR}^T]^{-1} \\
 &= \mathbf{A}\mathbf{s}(\mathbf{A}\mathbf{s})^T \mathbf{T}_{CR}^T [\mathbf{T}_{CR}\mathbf{A}\mathbf{s}(\mathbf{A}\mathbf{s})^T \mathbf{T}_{CR}^T]^{-1} \\
 &= \mathbf{A}\mathbf{\Sigma}_s \mathbf{A}^T \mathbf{T}_{CR}^T [\mathbf{T}_{CR}\mathbf{A}\mathbf{\Sigma}_s \mathbf{A}^T \mathbf{T}_{CR}^T]^{-1}
 \end{aligned} \tag{16}$$

References

- [1] S. Hu, M. Stead, G. Worrel, Automatic identification and removal of scalp reference signal for intracranial EEGs based on independent component analysis, *IEEE Trans. Biomed. Eng.* 54 (9) (2007) 1560–1572.
- [2] N. Madhu, R. Ranta, L. Maillard, L. Koessler, A unified treatment of the reference estimation problem in depth EEG recordings, *Med. Biol. Eng. Comput.* 50 (10) (2012) 1003–1015.
- [3] R. Ranta, N. Madhu, Reference estimation in EEG: Analysis of equivalent approaches, *IEEE Signal Process. Lett.* 19 (2012) 12–15.
- [4] Geselowitz D.B., The zero of potential, *IEEE Eng. Med. Biol. Mag.* 17 (1) (1998) 128–132.
- [5] J. Dien, Issues in the application of the average reference: review, critiques and recommendations, *Behav. Res. Methods Instrum. Comput.* 30 (1) (1998) 34–43.
- [6] D. Yao, A method to standardize a reference of scalp EEG recordings to a point at infinity, *Physiol. Meas.* 22 (2001) 693–711.
- [7] J. Kayser, C.E. Tenke, In search of the rosetta stone for scalp EEG, converging on reference-free techniques, *Clin. Neurophysiol. Off. J. Int. Fed. Clin. Neurophysiol.* 121 (2010) 1973–1975.
- [8] P.L. Nunez, R. Srinivasan, A.F. Westdorp, R.S. Wijesinghe, D.M. Tucker, R.B. Silberstein, P.J. Cadusch, EEG Coherency. I: Statistics, reference electrode, volume conduction, Laplacians, cortical imaging, and interpretation at multiple scales, *Electroencephalogr. Clin. Neurophysiol.* 103 (5) (1997) 499–515.
- [9] M. Essl, P. Rappelsberger, EEG coherence and reference signals: experimental results and mathematical explanations, *Med. Biol. Eng. Comput.* 39 (1998) 399–406.
- [10] P.L. Nunez, R.B. Silberstein, Z. Shi, M.R. Carpenter, R. Srinivasan, D.M. Tucker, S.M. Doran, P.J. Cadusch, R.S. Wijesinghe, EEG Coherency II: experimental comparisons of multiple measures, *Clin. Neurophysiol.* 110 (3) (1999) 469–486.
- [11] S. Hu, M. Stead, A.B. Gardner, G.A. Worrell, The effect of recording reference on eeg, phase synchrony and coherence, in: *Lecture Notes in Computer Science: Advances in Neural Networks*, Springer-Verlag, 2007, pp. 1273–1280.
- [12] S. Hu, M. Stead, Q. Dai, G. Worrell, On the recording reference contribution to EEG correlation, phase synchrony, and coherence, *IEEE Trans. Syst. Man Cybern. B* 40 (5) (2010) 1294–1304.
- [13] R. Salido-Ruiz, R. Ranta, V. Louis-Dorr, EEG montage analysis in the blind source separation framework, *Biomed. Signal Process. Control* 6 (1) (2011) 77–84.
- [14] Y. Zhai, D. Yao, A study on the reference electrode standardization technique for a realistic head model, *Comput. Methods Programs Biomed.* 76 (3) (2004) 229–238.
- [15] J. Yao, J.P. Dewald, Evaluation of different cortical source localization methods using simulated and experimental EEG data, *Neuroimage* 25 (2005) 369–382.
- [16] P. Nunez, REST: A good idea but not the gold standard, *Clin. Neurophysiol.* 121 (12) (2010) 2177–2180.
- [17] R. Salido-Ruiz, Problèmes inverses contraints en EEG: Applications aux potentiels absolus et à l'influence du signal de référence dans l'analyse de l'EEG (Ph.D. thesis), Université de Lorraine, 2012.
- [18] Q. Liu, J. Balsters, M. Baechinger, O. van der Groen, N. Wenderoth, D. Martini, Estimating a neutral reference for electroencephalographic recordings: The importance of using a high-density montage and a realistic head model, *J. Neural Eng.* 12 (5) (2015) 056012.
- [19] S. Hu, Y. Lai, P.A. Valdes-Sosa, M.L. Bringas-Vega, D. Yao, How do reference montage and electrodes setup affect the measured scalp EEG potentials? *J. Neural Eng.* 15 (2) (2018) 026013.
- [20] S. Hu, D. Yao, P.A. Valdes-Sosa, Unified Bayesian estimator of EEG reference at infinity: rREST (Regularized Reference Electrode Standardization Technique), *Front. Neurosci.* 12 (297) (2018).
- [21] S. Hu, D. Yao, M.L. Bringas-Vega, Y. Qin, P.A. Valdes-Sosa, The statistics of EEG unipolar references: Derivations and properties, *Brain Topogr.* (2019).
- [22] S. Baillet, J. Mosher, R. Leahy, Electromagnetic brain mapping, *IEEE Signal Process. Mag.* 18 (6) (2001) 14–30.
- [23] M. Libenson, *Practical Approach To Electroencephalography*, Elsevier Health Sciences, 2012.
- [24] B. Hjorth, An on-line transformation of EEG scalp potentials into orthogonal source derivations, *Electroencephalogr. Clin. Neurophysiol.* 39 (5) (1975) 526–530.
- [25] D. Yao, Y. Qin, S. Hu, L. Dong, M.L. Bringas Vega, P.A. Valdés Sosa, Which reference should we use for EEG and ERP practice? *Brain Topogr.* 32 (4) (2019) 530–549, <http://dx.doi.org/10.1007/s10548-019-00707>.
- [26] O. Bertrand, F. Perrin, J. Pernier, A theoretical justification of the average reference in topographic evoked potential studies, *Electroencephalogr. Clin. Neurophysiol.* 62 (1985) 462–464.
- [27] F.F. Offner, The EEG as potential mapping: The value of the average monopolar reference, *Electroencephalogr. Clin. Neurophysiol.* 2 (1–4) (1950) 213–214.
- [28] J.W. Osselson, Acquisition of EEG data by bipolar, unipolar and average reference methods: a theoretical comparison, *Electroencephalogr. Clin. Neurophysiol.* 19 (5) (1965) 527–528.
- [29] H. Hallel, B. Vanrumste, R. Grech, J. Muscat, W. De Clercq, A. Vergult, Y. D'Asseler, K. Camilleri, S. Fabri, S. Van Huffel, I. Lemahieu, Review on solving the forward problem in EEG source analysis, *J. Neuroeng. Rehabil.* (2007) 4–46.

- [30] K.B. Petersen, M.S. Pedersen, *The Matrix Cookbook*, Technical University of Denmark, 2012.
- [31] S. Baillet, J.C. Mosher, R.M. Leahy, D.W. Shattuck, Brainstorm: a matlab toolbox for the processing of MEG and EEG signals, *NeuroImage* 9 (1999) S246.
- [32] G. Korats, S. Cam, R. Ranta, M. Hamid, Applying ICA in EEG, choice of the window length and of the decorrelation method, in: J. Gabriel, J. Schier, S. van Huffel, E. Conchon, C. Correia, A. Fred, H. Gamboa (Eds.), *Biomedical Engineering Systems and Technologies*, in: *Communications in Computer and Information Science*, vol. 357, Springer, Berlin Heidelberg, 2013, pp. 269–286.
- [33] M. Stenroos, V. Mäntynen, J. Nenonen, A Matlab library for solving quasi-static volume conduction problems using the boundary element method, *Comput. Methods Progr. Biomed.* 88 (3) (2007) 256–263.
- [34] L. Koessler, L. Maillard, A. Benhadid, J.P. Vignal, J. Felblinger, H. Vespignani, M. Braun, Automated cortical projection of EEG sensors: anatomical correlation via the international 10–10 system, *Neuroimage* 46 (1) (2009) 64–72.
- [35] W. Menke, *Geophysical Data Analysis: Discrete Inverse Theory*, Academic Press, 2018.
- [36] J.W. Demmel, *Applied Numerical Linear Algebra*, vol. 56, SIAM, 1997.
- [37] L.N. Trefethen, D. Bau III, *Numerical Linear Algebra*, vol. 50, SIAM, 1997.
- [38] B. Noble, J. Daniel, *Applied Linear Algebra*, third ed., Englewood Cliffs, 1988.
- [39] F. Chella, V. Pizzella, F. Zappasodi, L. Marzetti, Impact of the reference choice on scalp EEG connectivity estimation, *J. Neural Eng.* 13 (3) (2016) 036016, URL: <http://stacks.iop.org/1741-2552/13/i=3/a=036016>.